



Estimating temporal and spatial variation of ocean surface $p\text{CO}_2$ in the North Pacific using a self-organizing map neural network technique

S. Nakaoka¹, M. Telszewski^{1,*}, Y. Nojiri¹, S. Yasunaka¹, C. Miyazaki^{1,**}, H. Mukai¹, and N. Usui²

¹National Institute for Environmental Studies, 16-2 Onogawa, Tsukuba, Ibaraki 305-8506, Japan

²Meteorological Research Institute, 1-1 Nagamine, Tsukuba, Ibaraki 305-0052, Japan

* now at: International Ocean Carbon Coordination Project, Institute of Oceanology of Polish Academy of Sciences, Ul. Powstańców Warszawy 55, 81-712 Sopot, Poland

** now at: Hokkaido University, Kita 8 Nishi 5, Kita-ku, Sapporo, Hokkaido 060-0810, Japan

Correspondence to: S. Nakaoka (nakaoka.shinichiro@nies.go.jp)

Received: 4 February 2013 – Published in Biogeosciences Discuss.: 8 March 2013

Revised: 25 June 2013 – Accepted: 9 August 2013 – Published: 26 September 2013

Abstract. This study uses a neural network technique to produce maps of the partial pressure of oceanic carbon dioxide ($p\text{CO}_2^{\text{sea}}$) in the North Pacific on a 0.25° latitude \times 0.25° longitude grid from 2002 to 2008. The $p\text{CO}_2^{\text{sea}}$ distribution was computed using a self-organizing map (SOM) originally utilized to map the $p\text{CO}_2^{\text{sea}}$ in the North Atlantic. Four proxy parameters – sea surface temperature (SST), mixed layer depth, chlorophyll *a* concentration, and sea surface salinity (SSS) – are used during the training phase to enable the network to resolve the nonlinear relationships between the $p\text{CO}_2^{\text{sea}}$ distribution and biogeochemistry of the basin. The observed $p\text{CO}_2^{\text{sea}}$ data were obtained from an extensive dataset generated by the volunteer observation ship program operated by the National Institute for Environmental Studies (NIES). The reconstructed $p\text{CO}_2^{\text{sea}}$ values agreed well with the $p\text{CO}_2^{\text{sea}}$ measurements, with the root-mean-square error ranging from $17.6\ \mu\text{atm}$ (for the NIES dataset used in the SOM) to $20.2\ \mu\text{atm}$ (for independent dataset). We confirmed that the $p\text{CO}_2^{\text{sea}}$ estimates could be improved by including SSS as one of the training parameters and by taking into account secular increases of $p\text{CO}_2^{\text{sea}}$ that have tracked increases in atmospheric CO_2 . Estimated $p\text{CO}_2^{\text{sea}}$ values accurately reproduced $p\text{CO}_2^{\text{sea}}$ data at several time series locations in the North Pacific. The distributions of $p\text{CO}_2^{\text{sea}}$ revealed by 7 yr averaged monthly $p\text{CO}_2^{\text{sea}}$ maps were similar to Lamont-Doherty Earth Observatory $p\text{CO}_2^{\text{sea}}$ climatology, allowing, however, for a more detailed analysis of biogeo-

chemical conditions. The distributions of $p\text{CO}_2^{\text{sea}}$ anomalies over the North Pacific during the winter clearly showed regional contrasts between El Niño and La Niña years related to changes of SST and vertical mixing.

1 Introduction

The ocean plays an important role as a major carbon reservoir for CO_2 emitted to the atmosphere from fossil fuel burning, cement production, and biomass burning. The ocean has absorbed about 48 % of the CO_2 emitted to the atmosphere by fossil fuel combustion since the Industrial Revolution (Sabine et al., 2004). To evaluate the global budget of oceanic CO_2 uptake, measurements of the partial pressure of CO_2 ($p\text{CO}_2^{\text{sea}}$) in surface seawater have been carried out over the global ocean, with the highest intensity in the equatorial Pacific (Feely et al., 1987, 2006; Ishii et al., 2009), the North Atlantic (Cooper et al., 1998; Olsen et al., 2003; Schuster et al., 2009), and the North Pacific (Inoue et al., 1995; Murphy et al., 2001a; Zeng et al., 2002; Chierici et al., 2006). A compilation of worldwide efforts to measure $p\text{CO}_2^{\text{sea}}$ on a global scale can be found in Takahashi et al. (2009). The authors, led by a team at the Lamont-Doherty Earth Observatory (LDEO), computed a 35 yr $p\text{CO}_2^{\text{sea}}$ climatology (for a reference year 2000) on 4° latitude \times 5° longitude resolution

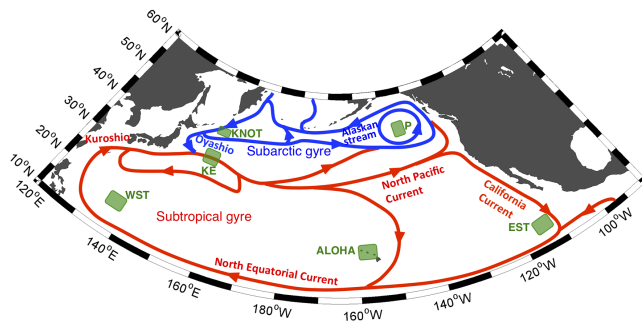


Fig. 1. Schematic map of the current system in the North Pacific rewritten from Schmitz (1996) with the areas of three ocean time-series stations and three areas for comparison of seasonal and interannual variations of $p\text{CO}_2^{\text{sea}}$ and related oceanic parameters. “KNOT”, “P”, and “ALOHA” denote ocean time-series station areas in the North Pacific, and “WST”, “KE”, and “EST” denote ocean areas of the western subtropics, Kuroshio Extension, and eastern subtropics, respectively.

and estimated the annual global air–sea CO_2 exchange at $-1.6 \pm 0.9 \text{ PgC yr}^{-1}$.

Neural network (NN) techniques can be generally described as empirical statistical tools that resolve, to a certain degree, the nonlinear and often discontinuous relationships among proxy parameters without any a priori assumptions. In the past decade a handful of authors have reported the application of an NN technique to basin-scale $p\text{CO}_2^{\text{sea}}$ analysis (e.g., Lefèvre et al., 2005; Jamet et al., 2007; Friedrich and Oschlies, 2009a, b; Telszewski et al., 2009), concentrating mainly on the North Atlantic Ocean. Most recently, Telszewski et al. (2009) successfully applied a self-organizing-map (SOM) based NN technique to reconstruct $p\text{CO}_2^{\text{sea}}$ distribution in the North Atlantic (10.5 to 75.5° N, 9.5° E to 75.5° W) for three years (2004 to 2006) by examining nonlinear/discontinuous relationship between $p\text{CO}_2^{\text{sea}}$ and ocean parameters of sea surface temperature (SST), mixed layer depth (MLD), and chlorophyll *a* concentration (CHL). One of the main benefits of this approach over the more traditional techniques, such as multiple linear regression (MLR), is that there are numerous empirical relationships established (e.g., 2220 in Telszewski et al., 2009) between examined parameters, allowing for more accurate representation of the highly variable system of interconnected water properties.

The North Pacific is dominated by two major current regimes: the subarctic and subtropical gyres (Fig. 1). The cold Oyashio Current and the warm Kuroshio Current are the western boundary currents of the North Pacific subarctic and subtropical gyres, respectively. The two currents meet at midlatitudes in the western North Pacific and turn toward the east as the North Pacific Current. The North Pacific has been typically characterized as a high-nutrient, low-chlorophyll region of the ocean at most of high latitudes because of the low influx of iron to the ocean surface (Dugdale

and Wilkerson, 1991), and as a low-nutrient, low-chlorophyll region at the western and central low latitudes (Karl and Letelier, 2008; Lin et al., 2011). The Bering Sea, which is a marginal sea of the North Pacific, and coastal regions are upwelling areas within which the transport of nutrient- and CO_2 -rich subsurface water to the surface assures high biological productivity (Chierici et al., 2006). In the North Pacific, there are expected to be thus quite large temporal and spatial variations of $p\text{CO}_2^{\text{sea}}$. Zeng et al. (2002) reported that large temporal amplitude of $\Delta p\text{CO}_2$ ($p\text{CO}_2^{\text{sea}} - p\text{CO}_2^{\text{air}}$) over $60 \mu\text{atm}$ was apparent in the western-central subarctic and the eastern subtropics based on their measurements between 1995 and 1999.

For analysis of temporal variability of $p\text{CO}_2^{\text{sea}}$ or $\Delta p\text{CO}_2$ in the North Pacific, Stephens et al. (1995) estimated basin-scale monthly $\Delta p\text{CO}_2$ distributions using simple linear regression analysis between $p\text{CO}_2^{\text{sea}}$ and SST in 1985. Recently, Sarma et al. (2006) used MLR analysis to estimate $p\text{CO}_2^{\text{sea}}$ from SST and satellite-based CHL observations in high-latitude regions of the eastern and western North Pacific, but the applicability of the MLR equations was limited to spring and summer. Takamura et al. (2010) also used MLR analysis to reconstruct $p\text{CO}_2^{\text{sea}}$ distributions as a function of SST and sea surface salinity (SSS) from 1999 to 2006 in mid-latitudes (25 to 40° N, 120 to 150° W, 140 to 170° E).

The precise time-series analyses of pelagic ocean $p\text{CO}_2^{\text{sea}}$ variability are limited to time-series stations (Bates, 2007, 2012; Dore et al., 2009; González-Dávila et al., 2010) where monthly $p\text{CO}_2^{\text{sea}}$ observations are available over extended time periods. Two areas of frequent shipboard observations of $p\text{CO}_2^{\text{sea}}$ other than time-series stations are the eastern and western equatorial Pacific (e.g., Feely et al., 2006; Ishii et al., 2009), where the observed interannual $p\text{CO}_2^{\text{sea}}$ variations are associated with the El Niño–Southern Oscillation (ENSO). Another place where there have been frequent shipboard $p\text{CO}_2^{\text{sea}}$ observations in the North Pacific is the 137° E repeat line (Midorikawa et al., 2006), where a weak but significant relationship between $p\text{CO}_2^{\text{sea}}$ and ENSO has been observed. A basin-wide analysis of observed $p\text{CO}_2^{\text{sea}}$ variability (including the analysis of the interannual signal) has not yet been successfully performed. An atmospheric CO_2 inverse model (Patra et al., 2005) and an ocean biogeochemical model (Valsala et al., 2012), however, suggest the possible correlation of the $p\text{CO}_2^{\text{sea}}$ variability with Pacific Decadal Oscillation (PDO).

Our goal in this study was to reconstruct temporal and spatial variability of the $p\text{CO}_2^{\text{sea}}$ distribution in the North Pacific for seven years from 2002 to 2008 using the SOM technique applied to the observational $p\text{CO}_2^{\text{sea}}$ dataset obtained by the NIES Volunteer Observing Ship (VOS) program. We then compared the estimated $p\text{CO}_2^{\text{sea}}$ values with measured $p\text{CO}_2^{\text{sea}}$ values obtained from the NIES VOS program and independent validation datasets in various areas of the North

Pacific (Fig. 1). We also presented the change of the $p\text{CO}_2^{\text{sea}}$ distribution in response to the ENSO events.

2 Method and datasets

2.1 Method of $p\text{CO}_2^{\text{sea}}$ estimation

The study area includes the North Pacific from 10 to 60° N and from 120° E to 90° W, and is hereafter called the North Pacific, although we have excluded coastal (bathymetric depth < 500 m) and ice-covered (SST < -1.8 °C) areas from the analysis. In this study, we hypothesized that $p\text{CO}_2^{\text{sea}}$ could be estimated by a linear function of time and an SOM function (f_{SOM}) of four independent variables: SST, MLD, CHL, and SSS. The equation for $p\text{CO}_2^{\text{sea}}$ then takes the following form:

$$p\text{CO}_2^{\text{sea}} = a \times (t - t_{\text{ref}}) + f_{\text{SOM}}(\text{SST, MLD, CHL, SSS}). \quad (1)$$

In Eq. (1) a is the secular rate of change of atmospheric CO_2 in $\mu\text{atm day}^{-1}$, t denotes the date, and the reference date t_{ref} is set to 30 June 2005. In addition, we assumed $p\text{CO}_2^{\text{sea}}$ to be a linear function of time in order to take into account the influence of anthropogenic CO_2 emissions on $p\text{CO}_2^{\text{sea}}$, an effect that could not be accounted for by SST, MLD, CHL, or SSS. The anthropogenic influence on $p\text{CO}_2^{\text{sea}}$ is considered negligible for relatively short analyses, e.g., three years (cf., Lefèvre et al., 2005; Telszewski et al., 2009), but it builds up to around 10 μatm after seven years. Midorikawa et al. (2006) reported that the secular trend of $p\text{CO}_2^{\text{sea}}$ varied from 1.3 to 1.8 $\mu\text{atm yr}^{-1}$ (close to the rate of increase of atmospheric CO_2) in the western subtropical North Pacific based on their measurements over 20 yr along 137° E. Wong et al. (2010) also reported that their 30 yr time series of measurements along Line P, the line connecting ocean station P (50° N, 145° W) to the coast, showed that the long-term trend of $p\text{CO}_2^{\text{sea}}$ tracked the increase of atmospheric CO_2 in the eastern subarctic region. Takahashi et al. (2006) concluded that, for the most part, the increase of oceanic CO_2 in the North Pacific followed the increase of atmospheric CO_2 for the last 35 yr with the increase rate varying geographically, reflecting differences in local oceanographic biogeophysical processes. We assumed in this study that the secular trend of $p\text{CO}_2^{\text{sea}}$ was approximately a constant fraction of the rate of change of atmospheric CO_2 over the North Pacific. Specifically, we assumed the value of the coefficient a in Eq. (1) to be 4.82×10^{-3} ($= 1.76/365.285$) $\mu\text{atm day}^{-1}$, which is the rate of increase of atmospheric CO_2 concentration converted from the CO_2 mole fractions ($x\text{CO}_2^{\text{air}}$) in the GLOBALVIEW- CO_2 dataset (GLOBALVIEW- CO_2 , 2011) for the North Pacific region during the period of analysis.

The method for reconstructing $p\text{CO}_2^{\text{sea}}$ is based on the methodology of Telszewski et al. (2009), but we allocated about three times as many neurons on a flat sheet map (53×115) to improve the estimate. A neuron in this study

is a vector that has four components: SST, MLD, CHL, and SSS. The values of these components, the training dataset, are prospectively normalized linearly (SST, SSS) or logarithmically (MLD, CHL) to create an even distribution among the input variables (cf., Fig. 3 of Telszewski et al., 2009). As indicated schematically in Fig. 2, three processes are executed in order to estimate basin-wide $p\text{CO}_2^{\text{sea}}$ fields in the SOM analysis procedure.

First, a neuron's weight vectors (x_i), which are linearly initialized, are repeatedly trained by input vectors (y_j), by being presented with the normalized SST, MLD, CHL, and SSS values, until the statistical composition of the training dataset is extracted and the neural network sufficiently represents the nonlinear interdependence of proxy parameters used in training (Training Process in Fig. 2a). At each step, Euclidean distances (D) are calculated between the weight vectors of neurons and the input vector:

$$D(x_i, y_j) = \left[(x_{i_{\text{SST}}} - y_{j_{\text{SST}}})^2 + (x_{i_{\text{MLD}}} - y_{j_{\text{MLD}}})^2 + (x_{i_{\text{CHL}}} - y_{j_{\text{CHL}}})^2 + (x_{i_{\text{SSS}}} - y_{j_{\text{SSS}}})^2 \right]^{0.5}. \quad (2)$$

The neuron closest to the training data point in Euclidean distance terms, here called the winner, is adjusted towards its value by a fraction of this distance dictated by the linearly time-decreasing learning function. At the same time, the neurons in the vicinity of the winner are also adjusted towards the value of the training data point by a fraction of the winner's adjustment in accordance with a time-decreasing Gaussian function, as explained by Kohonen (2001). This process results in clustering of similar neurons and self-organization of the map. The observed $p\text{CO}_2^{\text{sea}}$ dataset is not required at this stage of the analysis.

Second, each neuron is labeled with an observed $p\text{CO}_2^{\text{sea}}$ value. Technically, the labeling process follows the same principles as the training process. The labeling data, which in this study consist of the observed $p\text{CO}_2^{\text{sea}}$ value assigned to a reference year by adding/subtracting the assumed temporal change of $p\text{CO}_2^{\text{sea}}$ and coincided with normalized SST, MLD, CHL, and SSS values, is presented to the neural network, and a winner neuron is found (Labeling Process in Fig. 2b). Instead of adjusting the winner's value, it is labeled with the $p\text{CO}_2^{\text{sea}}$ value of the labeling data. This process is carried out for each of the observed $p\text{CO}_2^{\text{sea}}$ values. After the labeling process, most neurons are labeled with a $p\text{CO}_2^{\text{sea}}$ value. Neurons are consequently represented by five-dimensional vectors.

Third, the labeled SOM neurons are used to assign $p\text{CO}_2^{\text{sea}}$ values to the geographical grid points of the North Pacific (Mapping Process in Fig. 2c). The initial training dataset is presented to the trained and labeled SOM map. Upon computing the winner neuron, no adjustments are made. Instead, the training data are assigned a $p\text{CO}_2^{\text{sea}}$ value of the winner neuron. This value becomes a $p\text{CO}_2^{\text{sea}}$ estimate for time and location determined by the spatio/temporal coordinates

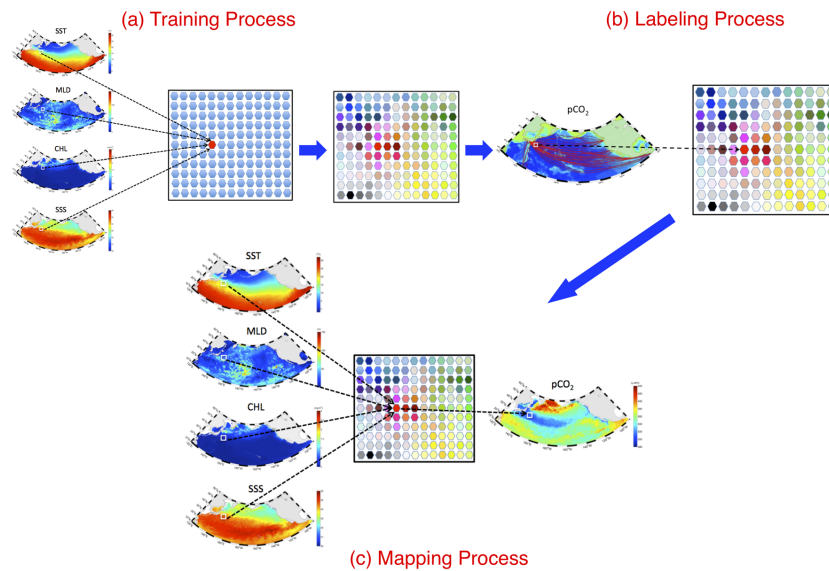


Fig. 2. Visualization of the processes that make up the procedure for SOM analysis.

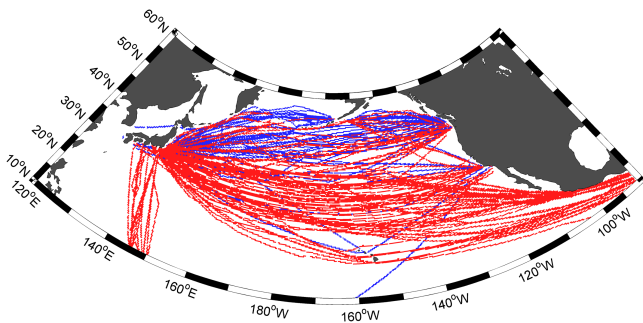


Fig. 3. Composite cruise tracks from 1998 to 2008. Blue lines represent the cruises from 1998 to 2001 and red lines show the cruises after 2002.

of each training datum after the temporal adjustment is done as expressed in Eq. (1).

Consequently, the $p\text{CO}_2^{\text{sea}}$ output produced in this work has originally daily frequency and 0.25° latitude \times 0.25° longitude resolution. The reconstructed monthly $p\text{CO}_2^{\text{sea}}$ distributions obtained as a result of this work will be available for scientific purposes from the NIES's Ship of Opportunity Program (SOOP) website: <http://soop.jp>.

2.2 Training dataset (SST, MLD, CHL, SSS)

We used four high-resolution datasets – one each for SST, MLD, CHL, and SSS – to train the SOM. We obtained observed SST datasets from the Merged satellite and in situ data Global Daily Sea Surface Temperatures (MGDSST) project (<http://goos.kishou.go.jp/rrtdb/database.html>) at a daily frequency and 0.25° latitude \times 0.25° longitude resolution (Kurihara et al., 2006). We obtained daily as-

simulated MLD estimates from the GLObal Ocean Reanalysis and Simulations (GLORYS) model by Mercator Ocean (Le Centre National de la Recherche Scientifique, France) with a horizontal resolution of 0.25° latitude \times 0.25° longitude (Bernard et al., 2006; Ferry et al., 2010). Satellite CHL data were obtained from MODIS-Aqua and SeaWiFS Level 3 Standard products provided by NASA/GFSC/DAAC at a frequency of eight per day and resolution of 9 km (<http://oceancolor.gsfc.nasa.gov>). We obtained assimilated SSS estimates from the MOVE/MRI.COM-NP model of the Meteorological Research Institute, Japan, at a frequency of 10 per day and horizontal resolution of 0.5° latitude and 0.5° longitude (Usui et al., 2006). For the analysis all parameters were re-gridded onto a frequency of one per day and horizontal resolution of 0.25° latitude \times 0.25° longitude.

We compared the assimilated datasets of SST and SSS with in situ measurements obtained by the NIES VOS project. The values of their differences were calculated to be about $0.01 \pm 0.53^\circ\text{C}$ and 0.03 ± 0.18 , respectively. O'Reilly et al. (2000) reported that the CHL difference between observed values and satellite-borne data was estimated to be 0.00 ± 0.25 , while the uncertainty of MLD estimate has not been reported. The above sources of uncertainty compose a fraction of the overhaul uncertainty of the method described in Sect. 2.7.1. In this study we have not attempted to assess the relative significance of various sources of uncertainty in the method.

2.3 $p\text{CO}_2^{\text{sea}}$ datasets for labeling

To estimate $p\text{CO}_2^{\text{sea}}$ fields in the North Pacific, it was necessary to label the trained SOM neurons with $p\text{CO}_2^{\text{sea}}$ values. In the labeling process, observed $p\text{CO}_2^{\text{sea}}$ data together with

Table 1. Summary of NIES surface ocean CO_2 measurements made by four volunteer observing ships in the Pacific Ocean.

Vessel name	Period	Observed area	NDIR analyzer
<i>M/S Skaugran</i>	Mar 1995–Sep 1999	North Pacific	Rosemount Analytical Model 880A
<i>M/S Alligator Hope</i>	Nov 1999–Mar 2001	North Pacific	Licor 6262
<i>M/S Pyxis</i>	Jul 2002–present	North Pacific	Licor 6262 (–Apr 2006) Licor 7000 (Apr 2006–)
<i>M/S Trans Future 5</i>	Jul 2006–present	Western North/ South Pacific	Licor 6262

corresponding SST, MLD, CHL, and SSS values were used. We utilized a subset of the North Pacific dataset collected by the NIES VOS program. The $p\text{CO}_2^{\text{sea}}$ data are available for public use from NIES's SOOP website: <http://soop.jp>. Information related to the four VOS lines is summarized in Table 1, and their composite cruise routes are depicted in Fig. 3. The commercial ships collaborating in the NIES VOS program have taken part in trans-Pacific cruises between Japan and North America (10 to 55° N, 140 to 230° E) since March 1995 and between Japan and Oceania (45° S to 35° N, 140 to 180° E) since July 2006. The ships sail regularly at intervals of about 5–8 weeks between Japan and North America or Oceania. On the North America route the volunteer ship sailed to the northern part of North America in the early part of the NIES VOS program, but since 2003 the route has occasionally shifted to the southeast to pass through the Panama Canal (Supplement Fig. 1). On the Oceania route the volunteer ship has sailed regularly on a biweekly basis, with the shipping route mostly fixed since July 2006.

Although we reconstructed $p\text{CO}_2^{\text{sea}}$ in the North Pacific after 2002, in the analysis we used some in situ data for years 1998–2001 due to the insufficient data coverage especially in the subarctic region for years 2002–2008. The addition of $p\text{CO}_2^{\text{sea}}$ data from 1998 to 2001 to the labeling dataset improved the coverage of monthly measurements (Supplement, Fig. 2). The improved coverage facilitated reproduction of the rapid drawdown of $p\text{CO}_2^{\text{sea}}$ due to phytoplankton photosynthesis during the spring bloom in the highly productive western mid–high latitude region.

Murphy et al. (2001b) and Fransson et al. (2006) have both described the technical intricacies of the ocean surface CO_2 measurement system used by the NIES VOS program; therefore we only outline the basics here. The nondispersive infrared analyzer used for those measurements was changed from a Licor 6262 to a Licor 7000 for the *M/S Pyxis* cruises in 2006 (Table 1). The CO_2 standard gases were calibrated by the NIES, and are traceable to the World Meteorological Organization scale. The flow-through tandem equilibrator provides a continuous $p\text{CO}_2^{\text{sea}}$ output with high temporal resolution (Murphy et al., 2001b). The $p\text{CO}_2^{\text{sea}}$ measurements were made every 10 s, and the $p\text{CO}_2^{\text{sea}}$ data were 10 min averages of those measurements. The $p\text{CO}_2^{\text{sea}}$ data were then

averaged on a daily basis within 0.25° latitude \times 0.25° longitude grid boxes. Consequently, the number of $p\text{CO}_2^{\text{sea}}$ data by the NIES VOS program amounted to 317 332, and a total of 73 284 $p\text{CO}_2^{\text{sea}}$ data were binned as the labeling dataset.

2.4 Other oceanic CO_2 datasets used for the validation of estimated $p\text{CO}_2^{\text{sea}}$

To validate $p\text{CO}_2^{\text{sea}}$ values reconstructed by the SOM analysis, we used the fugacity of oceanic CO_2 ($f\text{CO}_2^{\text{sea}}$) dataset from the Surface Ocean CO_2 Atlas (SOCAT: <http://www.socat.info>) version 1.5 database. That dataset has been in the public domain since September 2011, and has been subject to quality control as a part of an international collaboration of more than 10 institutes (including NIES) that work on ocean surface CO_2 observations (Pfeil et al., 2013). In the North Pacific, the SOCAT database contains the $f\text{CO}_2^{\text{sea}}$ values measured mainly by NIES, the Japan Meteorological Agency (JMA), the Japan Agency for Marine–Earth Science and Technology (JAMSTEC), and the United States National Oceanic and Atmospheric Administration (NOAA). For consistency with other datasets used in this study we recalculated $p\text{CO}_2^{\text{sea}}$ values from the obtained $f\text{CO}_2^{\text{sea}}$ (Pfeil et al., 2013) wherever necessary.

Underway $p\text{CO}_2^{\text{sea}}$ data and mooring $p\text{CO}_2^{\text{sea}}$ data collected by Wong and Johannessen (2010) and Sabine et al. (2010), respectively, were obtained from the Carbon Dioxide Information Analysis Center (CDIAC; <http://cdiac.ornl.gov/oceans/>). We used those data for the comparisons near ocean station P. In addition, we used $p\text{CO}_2^{\text{sea}}$ values calculated from measurements of dissolved inorganic carbon (DIC) and total alkalinity (TA) at two stations: station KNOT (44° N, 155° E, Wakita et al., 2010) and station ALOHA (23° N, 202° E, Dore et al., 2009).

2.5 Ranges of the training/labeling dataset

As explained by Telszewski et al. (2009), one of the biggest advantages of SOM analysis over the more traditional methods is the fact that the temporal and spatial distribution of proxy parameters in the training and labeling datasets does not influence the analysis. Instead ranges covered by these parameters in each dataset, and more precisely their relative

Table 2. Ranges of SST, MLD, CHL, and SSS in the training dataset, the labeling dataset, and the trained neurons. Percentages of the training data within the range of the labeling dataset and the neurons are given for each parameter.

	SST ($^{\circ}\text{C}$)			MLD (m)			CHL (mg m^{-3})			SSS (psu)		
	Min.	Max.	Cover (%)	Min.	Max.	Cover (%)	Min.	Max.	Cover (%)	Min.	Max.	Cover (%)
Training data	-1.8	32.7		1	> 500		0.00	10		30.15	35.69	
Labeling data	-1.1	31.5	99.940	1	416	99.995	0.00	10	100	30.15	35.69	100
Neurons	-0.6	29.4	96.651	1	194	99.807	0.00	3.2	99.778	31.79	35.58	99.886

overlap, determines whether the SOM will be able to reconstruct the distribution of the predicted parameter. Ranges of the training/labeling datasets and the trained neurons are summarized in Table 2. The training dataset SSTs varied between -1.8 and 32.7°C ; the MLD ranged from 1 m to more than 500 m; CHL varied from 0 to more than 10 mg m^{-3} ; and the range of SSS was 30.15–35.69. The values in the labeling datasets and neurons covered most of the range of values in the training dataset. However, the maximum MLDs in the labeling dataset (416 m) and in the neurons (194 m) were substantially lower than the maximum MLD in the training dataset (> 500 m, Table 2). Our results indicate that the correlation between $p\text{CO}_2^{\text{sea}}$ and MLD was not apparent when the MLD was deeper than 200 m (not shown), a result also reported for the North Atlantic by Telszewski et al. (2009). Therefore the MLD dataset is logarithmically normalized, aligning its weight during training (high weight in low values and low weight in high values) with its actual influence on the variability in $p\text{CO}_2^{\text{sea}}$. Such normalization means that the MLD change from 10 to 100 m is comparable (in terms of change of weight during training) to that from 100 to 1000 m.

2.6 Reconstructing $p\text{CO}_2^{\text{sea}}$ distributions in winter at high latitudes

The three products SST, MLD, and SSS provided full basin-wide coverage from 2002 to 2008. However, the CHL data were affected by the lack of satellite coverage from November to January at high latitudes of the North Pacific (north of 45°N) due to the low angle of the sun during that time and enormous atmospheric correction required to retrieve the signal. To reconstruct $p\text{CO}_2^{\text{sea}}$ for this area during those months, we assumed that $p\text{CO}_2^{\text{sea}}$ could be adequately characterized by only three parameters: SST, MLD, and SSS. The rationale for this assumption is that biological activity is relatively low during the winter at high latitudes (e.g., Imai et al., 2002). Therefore, we prepared another SOM trained by the three parameters SST, MLD, and SSS. We generated complete $p\text{CO}_2^{\text{sea}}$ maps in the study area by combining the $p\text{CO}_2^{\text{sea}}$ values obtained with the four-parameter SOM including CHL with the values obtained with the three-parameter SOM excluding CHL in the area north of 45°N (14 % of the study area) during the period from November to January. We calculated the difference between the $p\text{CO}_2^{\text{sea}}$ values estimated

with the four-parameter SOM and the three-parameter SOM during the above period in the region between 40 and 45°N and found it to be $-2.0 \pm 2.2\ \mu\text{atm}$. We added this difference to the $p\text{CO}_2^{\text{sea}}$ values obtained with the three-parameter SOM in the area north of 45°N .

2.7 Uncertainty and improvement of the $p\text{CO}_2^{\text{sea}}$ estimate

2.7.1 Uncertainty

For each in situ $p\text{CO}_2^{\text{sea}}$ measurement, the corresponding SOM $p\text{CO}_2^{\text{sea}}$ estimate was determined on the basis of the spatial (0.25° longitude \times 0.25° latitude grid) and temporal (daily intervals between 1 January 2002 and 31 December 2008) coordinates associated with the measurement. We calculated the root-mean-square error (RMSE) between observed $p\text{CO}_2^{\text{sea}}$ and estimated $p\text{CO}_2^{\text{sea}}$ values as follows:

$$\text{RMSE} = \sqrt{\frac{\sum (p\text{CO}_2^{\text{sea}}(\text{estimate}) - p\text{CO}_2^{\text{sea}}(\text{observed}))^2}{n}}, \quad (3)$$

where n is the number of points in the labeling dataset. The RMSE provided an estimate of the uncertainty of the method in reproducing the in situ measurements, and equaled $17.6\ \mu\text{atm}$, or 5.0 % of the average $p\text{CO}_2^{\text{sea}}$ of the in situ dataset. A scatter plot of the estimated $p\text{CO}_2^{\text{sea}}$ against the observed $p\text{CO}_2^{\text{sea}}$ (Fig. 4) shows that the values are clustered around the 1 : 1 line with slightly more scatter at very high $p\text{CO}_2^{\text{sea}}$. It should be noted that the reported RMSE is fairly large for some applications of small geographical extent such as determining air–sea CO_2 flux at local and regional scales.

As an independent validation exercise, we calculated the RMSE between the subset of the SOCAT dataset (all North Pacific data from 10 to 60°N and from 120°E to 90°W for 2002–2008 inclusive) and our SOM estimate. Such a calculated uncertainty estimate turns out to be $20.1\ \mu\text{atm}$, which makes this study similar to or more accurate than previous reports for the region, despite its largest temporal extent to date. Zeng et al. (2002) estimated the distribution of monthly averaged $p\text{CO}_2^{\text{sea}}$ in the North Pacific based on data from the NIES VOS program from 1995 to 1999, and reported that the estimated $p\text{CO}_2^{\text{sea}}$ agreed with the in situ $p\text{CO}_2^{\text{sea}}$ to within an RMSE of $24.9\ \mu\text{atm}$. Sarma et al. (2006) used an MLR method to estimate the distribution of monthly average

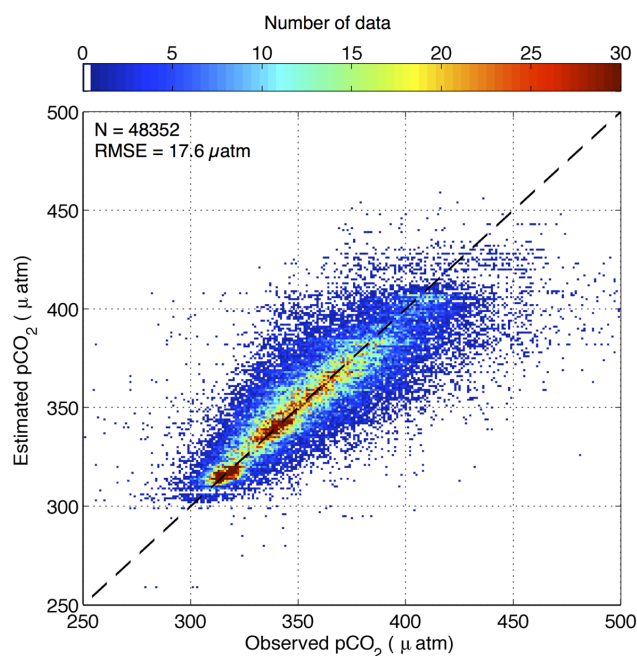


Fig. 4. Scatter plot of estimated $p\text{CO}_2^{\text{sea}}$ with observed $p\text{CO}_2^{\text{sea}}$. Colors indicate the number of data in a $1 \mu\text{atm} \times 1 \mu\text{atm}$ bin.

$p\text{CO}_2^{\text{sea}}$ in the North Pacific during the spring–summer period in 1998, and reported that the derived $p\text{CO}_2^{\text{sea}}$ agreed with the shipboard $p\text{CO}_2^{\text{sea}}$ observations to within an RMSE of 17–23 μatm .

2.7.2 Changes in the estimate scheme

We have implemented two major improvements over the previous attempt to utilize SOM neural network to compute the $p\text{CO}_2^{\text{sea}}$ distribution. In the first one, we followed the suggestion of Telszewski et al. (2009) and Friedrich and Oeschler (2009b) to use the SSS dataset as one of the training datasets to improve $p\text{CO}_2^{\text{sea}}$ estimates. The motivation behind using this parameter lies in the $p\text{CO}_2^{\text{sea}}$ dependence on (besides other factors) total alkalinity, which for most parts of the global ocean, including the North Pacific, can be accurately approximated from SSS. The SOM technique makes very good use of this relationship, and improvements in $p\text{CO}_2^{\text{sea}}$ estimates are seen throughout the basin and are especially apparent in high-gradient regions as described below. Moreover, inclusion of SSS in the SOM analysis may facilitate differentiation between temporal and spatial oceanic variability that could not be elucidated with only SST, MLD, and CHL.

To quantify the improvement achieved by using the SSS dataset, we generated another $p\text{CO}_2^{\text{sea}}$ map derived with a three-parameter SOM that excluded SSS and compared the result with the four-parameter SOM result. The RMSE between NIES dataset and the three-parameter SOM estimate was 20.0 μatm . Use of SSS in the training dataset therefore

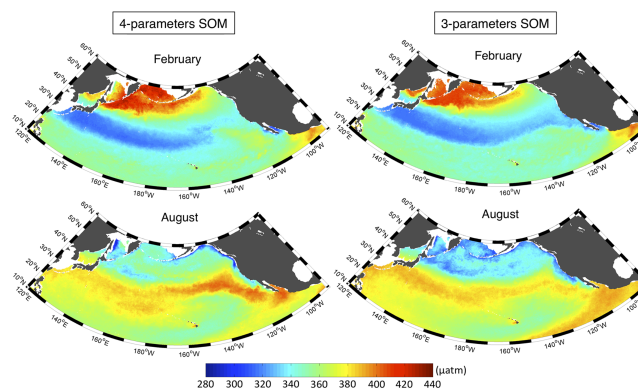


Fig. 5. Comparison of 7 yr averaged monthly $p\text{CO}_2^{\text{sea}}$ distributions from 2002 to 2008 in February (upper) and August (bottom). Figures on the left are the $p\text{CO}_2^{\text{sea}}$ distributions estimated from the four-parameter SOM including SSS. Figures on the right were estimated from the three-parameter SOM without SSS.

reduced the RMSE by 12%. The $p\text{CO}_2^{\text{sea}}$ distributions were also improved by the use of the SSS data. To visualize the differences, we mapped 7 yr averaged monthly $p\text{CO}_2^{\text{sea}}$ distributions in February and August derived with and without inclusion of SSS in the training dataset (Fig. 5). The estimated $p\text{CO}_2^{\text{sea}}$ derived from the three-parameter SOM in February is characterized by a smaller longitudinal difference in mid-latitudes than the $p\text{CO}_2^{\text{sea}}$ derived from the four-parameter SOM. Furthermore, use of the four-parameter SOM enabled reconstruction of quite high $p\text{CO}_2^{\text{sea}}$ values in August in the eastern low/midlatitude region, where the North Pacific Current flows, whereas use of the three-parameter SOM failed to reproduce this feature. Figure 6 shows the temporal variation of $p\text{CO}_2^{\text{sea}}$ derived with the two SOMs in the North Pacific Current region (36 to 38°N , 138 to 142°W). It clearly shows that the agreement between observed and estimated $p\text{CO}_2^{\text{sea}}$ values was better for the four-parameter SOM than the three-parameter SOM. The RMSE in the region was improved from 15.9 to 10.6 μatm by inclusion of SSS. The improvement was especially apparent during the summer, when high $p\text{CO}_2^{\text{sea}}$ values (about 400 μatm) were observed.

Taking into account the influence of anthropogenic CO_2 emissions on the trend of $p\text{CO}_2^{\text{sea}}$ was the second improvement introduced in this study. As described above it was done by adding or subtracting $1.76 \mu\text{atm yr}^{-1}$ ($4.82 \times 10^{-3} \mu\text{atm day}^{-1}$) to project observed $p\text{CO}_2^{\text{sea}}$ values to the $p\text{CO}_2^{\text{sea}}$ values in the reference year of 2005 (Eq. 1). The improvement of the $p\text{CO}_2^{\text{sea}}$ estimate by making this correction was not spatially uniform. For example, the RMSEs were reduced by adding the term from 10.2 to 9.1 μatm in the station P area (48 to 52°N , 142.5 to 147.5°W), from 8.8 to 7.4 μatm in the western subtropics (WST) area (14 to 18°N , 135.5 to 140.5°W), and from 10.8 μatm to 7.9 μatm in the station ALOHA area (21 to 25°N , 155.5 to 160.5°W). In contrast, the improvements at station KNOT area (43.5 to 45.5°N ,

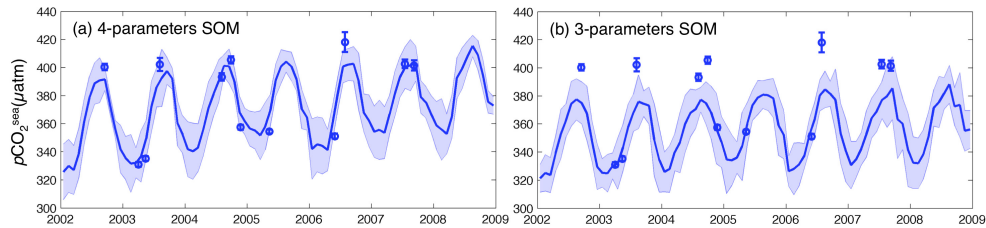


Fig. 6. The $p\text{CO}_2^{\text{sea}}$ variations in the area ($36\text{--}38^\circ\text{N}$, $138\text{--}142^\circ\text{W}$) where the North Pacific Current flows, estimated by the four-parameter SOM including SSS (a) and the three-parameter SOM without SSS (b). The blue lines and the shaded areas indicate the mean values of the estimated $p\text{CO}_2^{\text{sea}}$ and the spatial variability ($3\text{-}\sigma$) calculated in the area, respectively. Blue circles are the in situ $p\text{CO}_2^{\text{sea}}$ values obtained from the NIES VOS program. The $p\text{CO}_2^{\text{sea}}$ observations in the target areas include several grid points binned by 0.25° latitude \times 0.25° longitude resolution, and the bar indicates the spatial variability ($1\text{-}\sigma$).

153 to 157°E) and the Kuroshio Extension (KE) area (34 to 38°N , 155.5 to 160.5°E) were unclear (see in Fig. 1). These regions appear to be the same areas where the respective $p\text{CO}_2^{\text{sea}}$ trends are not close to that of atmosphere (Takahashi et al., 2006). This suggests that applying a basin-wide correction of $1.76\ \mu\text{atm}\ \text{yr}^{-1}$ ($4.82 \times 10^{-3}\ \mu\text{atm}\ \text{day}^{-1}$) might not be the most advantageous, and a nonuniform approach should be employed in the future where subregion-(province) specific correction should be calculated and applied. Overall in this study, inclusion of the secular trend effect slightly, but statistically significantly ($p < 0.05$), reduced the RMSE for the whole of the North Pacific.

3 Temporal and spatial variation of $p\text{CO}_2^{\text{sea}}$

3.1 Mapping of 7 yr averaged monthly $p\text{CO}_2^{\text{sea}}$ distributions

Figure 7 presents a comparison of 7 yr (2002–2008) averaged monthly $p\text{CO}_2^{\text{sea}}$ distributions derived from SOM results for February, May, August, and November with LDEO $p\text{CO}_2^{\text{sea}}$ climatology (Takahashi et al., 2009). The SOM-reconstructed $p\text{CO}_2^{\text{sea}}$ distributions in this study clearly show a tongue of very low $p\text{CO}_2^{\text{sea}}$ (about $320\ \mu\text{atm}$) water distributed (except in August) uniformly between the western and central midlatitude regions of the North Pacific (Fig. 7). Such low $p\text{CO}_2^{\text{sea}}$ values are attributed to high rates of photosynthesis (Kameda, 2003) and cooling of the seawater that occurred mainly in the subtropics. In addition, a band of relatively high $p\text{CO}_2^{\text{sea}}$ caused mainly by a seasonal rise in temperature was also apparent during the period from May to September in the western North Pacific between 15 and 30°N . The temperature rise began in April and amounted to about $2\text{--}5^\circ\text{C}$. Following the temperature dependence of $p\text{CO}_2^{\text{sea}}$ given by Takahashi et al. (1993), $\delta\ln p\text{CO}_2^{\text{sea}}/\delta T = 0.0423\ ^\circ\text{C}^{-1}$, the expected $p\text{CO}_2^{\text{sea}}$ rise due to the temperature effect is about $30\text{--}70\ \mu\text{atm}$. The observed increase in expected $p\text{CO}_2^{\text{sea}}$ is only about half of the expected $p\text{CO}_2^{\text{sea}}$ rise due to temperature effects. The in-

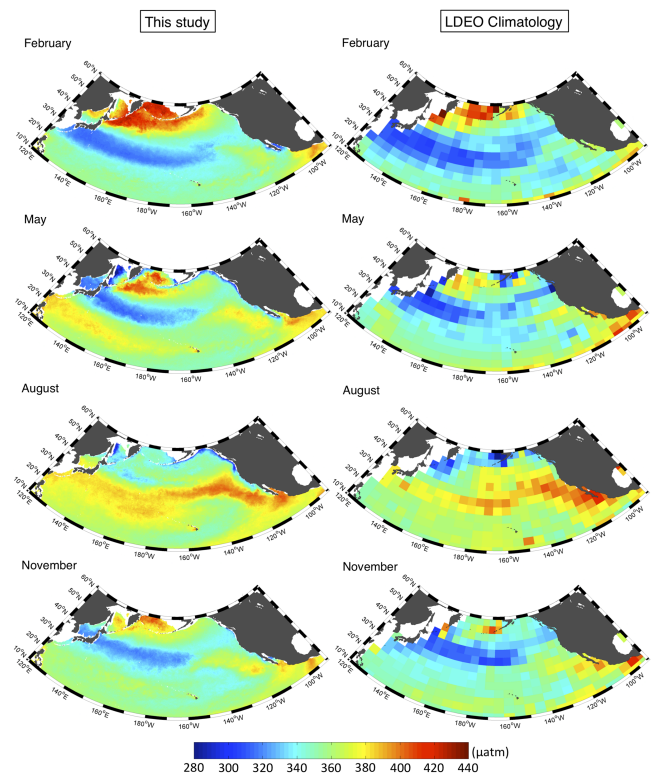


Fig. 7. Distributions of the 7 yr averaged monthly mean $p\text{CO}_2^{\text{sea}}$ in this study (panels on the left) and the LDEO monthly $p\text{CO}_2^{\text{sea}}$ climatology (panels on the right, but with $8.8\ \mu\text{atm}$ added to the maps to change the reference year from 2000 to 2005) for February, May, August, and November.

crease may have been attenuated by other factors such as photosynthetic uptake of CO_2 .

The comparison with the LDEO climatology shows that the SOM-reconstructed $p\text{CO}_2^{\text{sea}}$ maps reveal similar large-scale patterns to these known from the LDEO climatology. However, the SOM results, due to its much higher spatio-temporal resolution, allow for more detailed analysis of local and regional features. Both studies show high $p\text{CO}_2^{\text{sea}}$

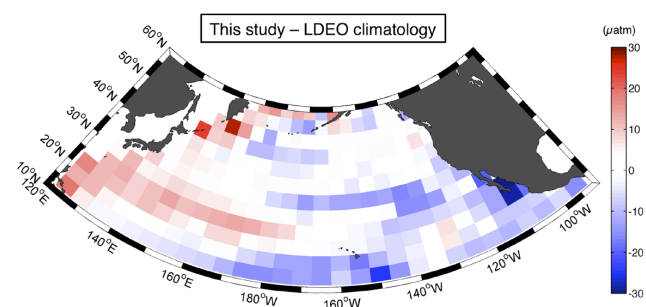


Fig. 8. Difference of the $p\text{CO}_2^{\text{sea}}$ between the 7 yr mean $p\text{CO}_2^{\text{sea}}$ in this study and the LDEO monthly $p\text{CO}_2^{\text{sea}}$ climatology (but with $8.8 \mu\text{atm}$ added to change the reference year from 2000–2005). Positive values indicate higher $p\text{CO}_2^{\text{sea}}$ in this study compared with the LDEO climatology.

values (over $400 \mu\text{atm}$) at high latitudes in the North Pacific in February; however, the SOM-reconstructed $p\text{CO}_2^{\text{sea}}$ distribution shows $p\text{CO}_2^{\text{sea}}$ -rich water between the Bering Sea and the coast of northern Japan along the axis of the cold, southward-flowing Eastern Kamchatka Current. As described in Sect. 2.7.2, high $p\text{CO}_2^{\text{sea}}$ values are apparent from June to October in the eastern low/midlatitude region, where the North Pacific Current and the California Current flow, and the high $p\text{CO}_2^{\text{sea}}$ field dominates. With respect to the coastal region, low estimates of $p\text{CO}_2^{\text{sea}}$ stretch along the coastline from the Aleutian Islands to the California Peninsula from May to October, when the concentration of phytoplankton is high.

The map of differences between SOM results and LDEO climatology for reference year 2005 is shown in Fig. 8. The difference distribution is positive in the western subarctic and the western subtropics and negative in the central-eastern subtropics, the calculated monthly mean difference is close to zero ($-0.8 \mu\text{atm}$), and its standard deviation is $11.2 \mu\text{atm}$.

3.2 Reproducibility of temporal $p\text{CO}_2^{\text{sea}}$ variations in each of six regions

To facilitate a discussion about the temporal variations of $p\text{CO}_2^{\text{sea}}$ in the North Pacific, Fig. 9 shows the time series of area-averaged $p\text{CO}_2^{\text{sea}}$ estimated in this study for six specific regions of the North Pacific along with observations made during several campaigns at these locations as well as computed estimates of Takamura et al. (2010). The grid size of all the averaged areas except in the station KNOT area is set to 4° latitude \times 5° longitude, whereas the station KNOT area is set to 43.5 – 44.5° N, 153 – 157° E to exclude the transition zone between the Kuroshio and the Oyashio. The estimated $p\text{CO}_2^{\text{sea}}$ values at each location generally agree well with observed values and other estimates, with most of the data lying within the spatial variability (triple the spatial standard deviation: $3\text{-}\sigma$) calculated for each area. However disagreements greater than $20 \mu\text{atm}$ between estimated $p\text{CO}_2^{\text{sea}}$

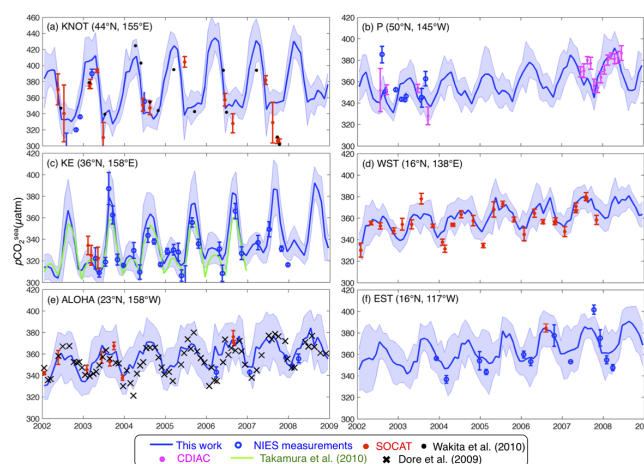


Fig. 9. Interannual variation of $p\text{CO}_2^{\text{sea}}$ (μatm) within time-series station areas and within ocean areas. The blue solid lines and shaded areas show the monthly $p\text{CO}_2^{\text{sea}}$ values and the spatial variability ($3\text{-}\sigma$) calculated in the respective areas. The grid size of all the averaged areas except in the station KNOT area is set to 4° latitude \times 5° longitude, whereas the station KNOT area is set to 43.5 – 45.5° N, 153 – 157° E. Blue circles and red dots are in situ $p\text{CO}_2^{\text{sea}}$ values obtained from NIES measurements and the SOCAT database, respectively. Black dots and crosses on panel (a) and (c) are the $p\text{CO}_2^{\text{sea}}$ values calculated from measurements of DIC and TA reported by Wakita et al. (2010) and Dore et al. (2009), respectively. Purple dots on panel (b) are the $p\text{CO}_2^{\text{sea}}$ values observed by Wong and Johannessen (2010) and Sabine et al. (2010). In panel (c), the solid green line denotes the $p\text{CO}_2^{\text{sea}}$ values during the 2002–2006 period estimated by Takamura et al. (2010). Note that the range of the ordinate in the station KNOT area is larger than those of other station areas.

and observed $p\text{CO}_2^{\text{sea}}$, as exemplified in the area surrounding station KNOT (Fig. 9a), occur occasionally, but there is no systematic overestimate by the SOM in this region. The calculated $p\text{CO}_2^{\text{sea}}$ in station P area generally agree well with the data from the NIES VOS program as well as with $p\text{CO}_2^{\text{sea}}$ values measured by an underway system from 2002 to 2003 and by a moored buoy system from 2007 to 2008 (Fig. 9b). The largest seasonal amplitudes tend to coincide with the largest disagreements between the estimates (Zeng et al., 2002). The calculated $p\text{CO}_2^{\text{sea}}$ values in the KE area of the eastern midlatitude region (Fig. 9c) agree well with the NIES dataset as well as with the $f\text{CO}_2^{\text{sea}}$ values from the SOCAT dataset, with all $p\text{CO}_2^{\text{sea}}$ values lying within the spatial variability. The results of Takamura et al. (2010) also agree with the $p\text{CO}_2^{\text{sea}}$ measurements to within 15 – $20 \mu\text{atm}$, and the temporal pattern of those data is generally consistent with the $p\text{CO}_2^{\text{sea}}$ estimates within the spatial variability from this study. The temporal variations of $p\text{CO}_2^{\text{sea}}$ in the WST (Fig. 9d) and station ALOHA area (Fig. 9e) agree well with the $p\text{CO}_2^{\text{sea}}$ values in the SOCAT dataset, even though the observed $p\text{CO}_2^{\text{sea}}$ data used for the labeling process in the SOM analysis rarely existed in these areas. The calculated

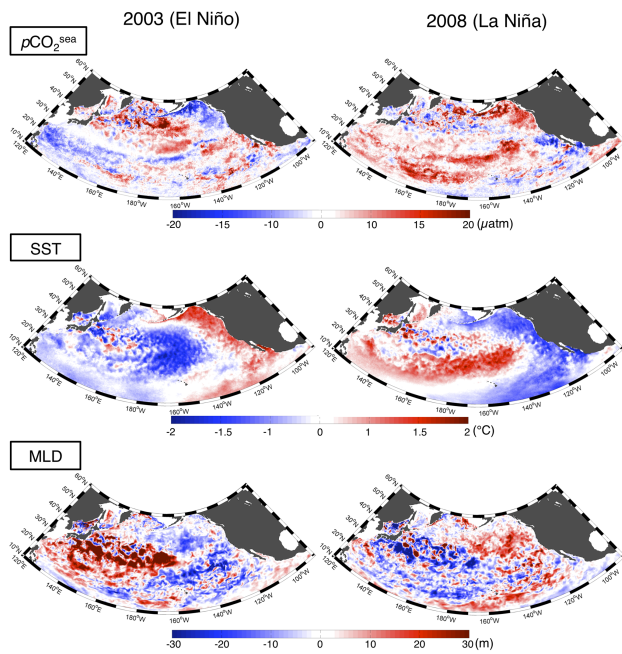


Fig. 10. Anomalies from the monthly climatology for the period box 2002–2008 for detrending $p\text{CO}_2^{\text{sea}}$ (upper), SST (middle), and MLD (bottom) distributions during the winter of 2003 (panels on the left) and 2008 (panels on the right).

$p\text{CO}_2^{\text{sea}}$ values in the eastern subtropics (EST) area (14 to 18° N, 115.5 to 119.5° W) also agree well with the data from the NIES VOS program (Fig. 9f). As shown in Fig. 9d–f, the patterns of variation were similar in the WST, station ALOHA, and EST areas. Keeping in mind that only data obtained by the NIES VOS program were used in the SOM labeling process, these results suggest that the labeling process allows for labeled SOM neurons to effectively learn $p\text{CO}_2^{\text{sea}}$ variations from $p\text{CO}_2^{\text{sea}}$ values observed in other subtropical areas. This confirms the earlier suggestions that the SOM technique, to a larger extent than more traditional mapping techniques, overcomes problems associated with temporal and spatial scarcity of the labeling data (in situ) by putting significant weight on the availability and quality of the training data (satellite and assimilation).

Finally, as an additional independent validation exercise, we calculated the RMSE between all the independent data visualized in Fig. 9 and equivalent SOM estimates. Such a calculated uncertainty estimate turns out to be 20.1 μatm , almost identical to that obtained for SOCAT dataset, giving more confidence in our error estimate.

3.3 Difference of $p\text{CO}_2^{\text{sea}}$ distributions during ENSO events

The ENSO has a large influence on the climate of the North Pacific (IPCC, 2007), and large fluctuations of $p\text{CO}_2^{\text{sea}}$ coincided with the ENSO cycle have also been observed in the

equatorial Pacific (Feely et al., 2006; Ishii et al., 2009). Based on their measurements from 1983 to 2003, Midorikawa et al. (2006) have suggested that the interannual variation of $p\text{CO}_2^{\text{sea}}$ in the western subtropical North Pacific is also related to the ENSO. Although the extent of the ENSO influence on oceanic and atmospheric variables is known to be global (Trenberth and Caron, 2000), the impact of the ENSO on the distribution of $p\text{CO}_2^{\text{sea}}$ over the entire area of the North Pacific is not well understood. Figure 10 depicts the estimated distributions of the detrended $p\text{CO}_2^{\text{sea}}$, SST, and MLD anomalies during the winters of 2003 (i.e., El Niño) and 2008 (i.e., La Niña). Anomalies in Fig. 10 are deviations from the monthly climatology for the period of 2002–2008. El Niño/La Niña periods were chosen in accordance with JMA's definition based on the 5-month running mean SST deviation for the NINO.3 region (5° S to 5° N, 90 to 150° W).

The patterns of SST anomalies in Fig. 10 are typical of El Niño and La Niña winters (Trenberth and Caron, 2000; Alexander et al., 2002). The $p\text{CO}_2^{\text{sea}}$ anomaly related to ENSO events is easily discernible in the western-central subtropical region, in the eastern subarctic region, and in the eastern midlatitude region south of 30° N. For example, a negative $p\text{CO}_2^{\text{sea}}$ anomaly is apparent in the western-central subtropical region in 2003 (El Niño), when the SST anomaly was negative, whereas a positive $p\text{CO}_2^{\text{sea}}$ anomaly is apparent in 2008 (La Niña), when the SST anomaly is positive. The opposite pattern is observed for the eastern midlatitude region south of 30° N. The amplitudes of the associated $p\text{CO}_2^{\text{sea}}$ anomalies are about 15 μatm , and their SST amplitudes are 1 °C. The $p\text{CO}_2^{\text{sea}}$ change closely tracked the SST change in accordance with the iso-chemical temperature dependency of Takahashi et al. (1993).

A negative relationship between $p\text{CO}_2^{\text{sea}}$ and SST is apparent in the eastern subarctic North Pacific, where the signal of thermodynamic changes on variations of $p\text{CO}_2^{\text{sea}}$ was opposite to that seen in the subtropics. As indicated in Fig. 10, the MLD anomaly clearly showed the typical pattern of ENSO events (Alexander et al., 2002), and the MLD was approximately 10 m deeper in 2008 than in 2003 in the region. CLIVAR Repeat Section Line P data provided by Miller et al. (2010) showed that surface (< 10 m) DIC concentration in station P in February 2003 is about 35 $\mu\text{mol kg}^{-1}$ lower than in February 2008. By using CO2SYS program (Lewis and Wallace, 1998; Robbins et al., 2010), the estimated $p\text{CO}_2^{\text{sea}}$ difference between February 2003 and February 2008 in the region caused by the changes of surface DIC, TA, temperature and salinity, is about 14 μatm . Since the $p\text{CO}_2^{\text{sea}}$ difference between 2002 and 2008 based on the DIC measurements is well consistent with the difference derived by the SOM results, it strongly suggests that more CO_2 -rich subsurface water was entrained into surface waters during the La Niña period than during the El Niño period.

4 Summary

In this study we used the SOM technique of Telszewski et al. (2009) to examine the temporal and spatial variations of $p\text{CO}_2^{\text{sea}}$ in the North Pacific during the period 2002–2008. To improve the $p\text{CO}_2^{\text{sea}}$ estimates, we used SSS as an additional training parameter and assumed a trend of increasing $p\text{CO}_2^{\text{sea}}$ to take into account the effect of anthropogenic CO_2 emissions on $p\text{CO}_2^{\text{sea}}$. The estimated results revealed that the SOM technique could satisfactorily reconstruct variations of $p\text{CO}_2^{\text{sea}}$ associated with bio-geophysical processes expressed by the variability in four proxy parameters: SST, MLD, CHL, and SSS. We calculated the uncertainty of the $p\text{CO}_2^{\text{sea}}$ estimation to be from $17.8\ \mu\text{atm}$ for the NIES labeling dataset to $20.2\ \mu\text{atm}$ for the SOCAT dataset. The fact that the uncertainty was reduced by about 12% by inclusion of SSS in the training dataset suggests that SSS can be a useful parameter for the estimation of temporal and spatial variation of $p\text{CO}_2^{\text{sea}}$. We also found that $p\text{CO}_2^{\text{sea}}$ estimates were improved by taking account of the temporal trend associated with anthropogenic CO_2 emissions.

The calculated $p\text{CO}_2^{\text{sea}}$ variations in six ocean areas generally agreed well not only with the NIES VOS program $p\text{CO}_2^{\text{sea}}$ data used for the labeling process but also with other in situ $p\text{CO}_2^{\text{sea}}$ datasets. Seven-year (2002–2008) averaged monthly $p\text{CO}_2^{\text{sea}}$ distributions were similar to 35 yr climatology $p\text{CO}_2^{\text{sea}}$ distributions (Takahashi et al., 2009). However, the SOM-based $p\text{CO}_2^{\text{sea}}$ mapping, with its high spatial resolution, reflected oceanic conditions with more detail. The estimated interannual $p\text{CO}_2^{\text{sea}}$ variability revealed a difference in the spatial pattern of $p\text{CO}_2^{\text{sea}}$ during the winter of the El Niño period in 2003 and the La Niña period in 2008. A negative $p\text{CO}_2^{\text{sea}}$ anomaly was apparent in 2003 in the western subtropical North Pacific and in the eastern subarctic North Pacific off the coast of Alaska, whereas a positive anomaly was apparent in 2008 in the same regions. In the western subtropical and eastern midlatitude regions, the correlation of the $p\text{CO}_2^{\text{sea}}$ variability with ENSO events seemed to be related mainly to changes in the thermodynamic properties of seawater. In contrast, similar correlation in the subarctic North Pacific seemed to be related to changes in vertical transport of CO_2 -rich subsurface waters.

Further improvement of $p\text{CO}_2^{\text{sea}}$ estimates will most certainly require an increase in the number of data points used for labeling. With new datasets becoming available (SOCAT version 2 and LDEO V2012) and offering relatively dense annual data coverage in several oceans regions, we are now in a position to commence a sensitivity study allowing for a meaningful quantitative assessment to be made of the uncertainty related to the amount of labeling data utilized during the mapping process. In this study, 7% of the neurons were not labeled, suggesting that in situ measurements covering a wider range of environmental conditions (as approximated by SST, MLD, CHL, and SSS) are needed to enable the full mapping potential of the method. We plan to undertake a

longer-term study covering global ocean using the community quality-controlled (Pfeil et al., 2013) SOCAT collection as the labeling dataset. This work will include a sensitivity study hopefully allowing for quantification of the relationship between the amount of the in situ data and the method's uncertainty estimate.

The number of neurons is also crucial for accurate $p\text{CO}_2^{\text{sea}}$ estimation. In this study we used three times as many neurons as Telszewski et al. (2009) to achieve adequate reproducibility of the $p\text{CO}_2^{\text{sea}}$ estimates. However, the number of neurons used in this study was based on the available computing power rather than determined by scientific need. It might also be possible to improve the $p\text{CO}_2^{\text{sea}}$ estimate by inclusion of more ocean parameters. Sea surface height is a potential training parameter with basin-wide coverage.

In addition to estimates in the North Pacific, long-term global $p\text{CO}_2^{\text{sea}}$ mapping based on such measurements is also important for understanding interannual variations of air–sea CO_2 exchanges. Although $p\text{CO}_2^{\text{sea}}$ variations related to climate changes such as the PDO have been reported (Valsala et al., 2012), the overall impact of such changes on global $p\text{CO}_2^{\text{sea}}$ variations is not well understood. In the present study, the study area was confined to the North Pacific. However, the SOM technique used in the present study has the potential to estimate $p\text{CO}_2^{\text{sea}}$ in regions where there are insufficient numbers of observations, and such regions will be our next target. It is axiomatic to say that further $p\text{CO}_2^{\text{sea}}$ measurements are critical, especially in the South Pacific, where few $p\text{CO}_2^{\text{sea}}$ measurements have been made (Sabine et al., 2013).

Supplementary material related to this article is available online at <http://www.biogeosciences.net/10/6093/2013/bg-10-6093-2013-supplement.pdf>.

Acknowledgements. We deeply appreciate the generous cooperation of Seaboard International Shipping Co., Mitsui O. S. K. Lines Co., Toyofuji Shipping Co., and Kagoshima Senpaku Co. with the NIES VOS program. We would like to thank the crew of the *M/S Skaugran*, *M/S Alligator Hope*, *M/S Pyxis*, and *M/S Trans Future 5*. We also thank S. Kariya and T. Yamada of the Global Environmental Forum for their constant assistance with the observations, and appreciate the work of K. Katsumata for calibrating the CO_2 standard gases. We are thankful to contributors of the SOCAT database and the CDIAC database for providing oceanic CO_2 data. We gratefully acknowledge Mercator Ocean for providing the GLORYS model output. The research was financially supported by the Global Environment Research Account for National Institutes by the Ministry of Environment, Japan. Finally, we also express our deep thanks to R. Wannikhof, A. Lenton, and two anonymous reviewers, who provided us with many useful comments.

Edited by: F. Chai

References

- Alexander, M. A., Blade, I., Newman, M., Lanzante, J. R., Lau, N.-C., and Scott, J. D.: The atmospheric bridge: The influence of ENSO teleconnections on air-sea interaction over the global oceans, *J. Climate*, 15, 2205–2231, 2002.
- Bates, N. R.: Interannual variability of the oceanic CO_2 sink in the subtropical gyre of the North Atlantic Ocean over the last 2 decades, *J. Geophys. Res.*, 112, C09013, doi:10.1029/2006JC003759, 2007.
- Bates, N. R., Best, M. H. P., Neely, K., Garley, R., Dickson, A. G., and Johnson, R. J.: Detecting anthropogenic carbon dioxide uptake and ocean acidification in the North Atlantic Ocean, *Biogeosciences*, 9, 2509–2522, doi:10.5194/bg-9-2509-2012, 2012.
- Bernard, B., Madec, G., Penduff, T., Molines, J.-M., Treguier, A.-M., Sommer, J. L., Beckmann, A., Biastoch, A., Böning, C., Dengg, J., Derval, C., Durand, E., Gulev, S., Remy, E., Talandier, C., Theetten, S., Maltrud, M., McClean, J., and Cuevas, B. D.: Impact of partial steps and momentum advection schemes in a global ocean circulation model at eddy-permitting resolution, *Ocean Dynam.*, 56, 543–567, doi:10.1007/s10236-006-0082-1, 2006.
- Cooper, D. J., Watson, A. J., and Ling, R. D.: Variation of $p\text{CO}_2$ along a North Atlantic shipping route (UK to the Caribbean): a year of automated observations., *Mar. Chem.*, 72, 151–169, 1998.
- Chierici, M., Fransson, A., and Nojiri, Y.: Biogeochemical processes as drivers of surface fCO_2 in contrasting provinces in the subarctic North Pacific Ocean, *Global Biogeochem. Cy.*, 20, GB1009, doi:10.1029/2004GB002356, 2006.
- Dore, J. E., Lukas, R., Sadler, D. W., Church, M. J., and Karl, D. M.: Physical and Biogeochemical Modulation of Ocean Acidification in the Central North Pacific, *PNAS*, 106, 12235–12240, doi:10.1073/pnas.0906044106, 2009.
- Dugdale, R. C. and Wilkerson, F. P.: Low specific nitrate uptake rate: A common feature of high-nutrient, low-chlorophyll marine ecosystems, *Limnol. Oceanogr.*, 36, 1678–1688, 1991.
- Feely, R. A., Gammon, R. H., Taft, B. A., Pullen, P. E., Waterman, L. S., Conway, T. J., Gendron, J. F., and Wisegarver, D. P.: Distribution of chemical tracers in the eastern Equatorial Pacific during and After the 1982–83 El Niño/Southern Oscillation Event, *J. Geophys. Res.*, 92, 6545–6558, 1987.
- Feely, R. A., Takahashi, T., Wanninkhof, R., McPhaden, M. J., Cosca, C. E., Sutherland, S. C., and Carr, M.-E.: Decadal variability of the air-sea CO_2 fluxes in the equatorial Pacific Ocean, *J. Geophys. Res.*, 111, C08S90, doi:10.1029/2005JC003129, 2006.
- Ferry, N., Parent, L., Garric, G., Barnier, B., Jourdain, N. C., and the Mercator Ocean team: Mercator Global Eddy Permitting Ocean Reanalysis GLORYS1V1: Description and Results, *Mercator Ocean Quarterly Newsletter*, 36, 15–27, 2010.
- Fransson, A., Chierici, M., and Nojiri, Y.: Increased net CO_2 outgassing in the upwelling region of the southern Bering Sea in a period of variable marine climate between 1995 and 2001, *J. Geophys. Res.*, 111, C08008, doi:10.1029/2004JC002759, 2006.
- Friedrich, T. and Oschlies, A.: Neural network-based estimates of North Atlantic surface $p\text{CO}_2$ from satellite data: A methodological study, *J. Geophys. Res.*, 114, C03020, doi:10.1029/2007JC004646, 2009a;
- Friedrich, T. and Oschlies, A.: Basin-scale $p\text{CO}_2$ maps estimated from ARGO float data: A model study, *J. Geophys. Res.*, 114, C10012, doi:10.1029/2009JC005322, 2009b.
- GLOBALVIEW-CO2: Cooperative Atmospheric Data Integration Project – Carbon Dioxide, CD-ROM, NOAA ESRL, Boulder, Colorado [Also available on Internet via anonymous FTP to ftp.cmdl.noaa.gov, Path: ccg/co2/GLOBALVIEW], 2011.
- González-Dávila, M., Santana-Casiano, J. M., Rueda, M. J., and Llinás, O.: The water column distribution of carbonate system variables at the ESTOC site from 1995 to 2004, *Biogeosciences*, 7, 3067–3081, doi:10.5194/bg-7-3067-2010, 2010.
- Imai, K., Nojiri, Y., Tsurushima, N., and Saino, T.: Time series of seasonal variation of primary productivity at station KNOT (44°N , 155°E) in the sub-arctic western North Pacific, *Deep-Sea Res. II*, 49, 5395–5408, 2002.
- Inoue, H. Y., Matsueda, H., Ishii, M., Fushimi, K., Hirota, M., Asanuma, I., and Takasugi, Y.: Long-term trend of the partial pressure of carbon dioxide ($p\text{CO}_2$) in surface waters of the western North Pacific 1984–1993, *Tellus B*, 47, 391–413, 1995.
- IPCC: Climate Change 2007: The Physical Science Basis. Contribution of Working Group I to the Fourth Assessment Report of the Intergovernmental Panel on Climate Change, edited by: Solomon, S., Qin, D., Manning, M., Chen, Z., Marquis, M., Averyt, K. B., Tignor, M., and Miller, H. L., Cambridge University Press, Cambridge, United Kingdom and New York, NY, USA, 2007.
- Ishii, M., Inoue, H. Y., Midorikawa, T., Saito, S., Tokieda, T., Sasano, D., Nakadate, A., Nemoto, K., Metzl, N., Wong, C. S., and Feely, R. A.: Spatial variability and decadal trend of the oceanic CO_2 in the western equatorial Pacific warm/fresh water, *Deep-Sea Res. II*, 56, 591–606, doi:10.1016/j.dsr2.2009.01.002, 2009.
- Jamet, C., Moulin, C., and Lefèvre, N.: Estimation of the oceanic $p\text{CO}_2$ in the North Atlantic from VOS lines in-situ measurements: parameters needed to generate seasonally mean maps, *Ann. Geophys.*, 25, 2247–2257, 2007, <http://www.ann-geophys.net/25/2247/2007/>.
- Kameda, T.: Studies on oceanic primary production using ocean color remote sensing data, *Bull. Fish. Res. Agen.*, 9, 118–148, 2003.
- Karl, D. M. and Letelier, R. M.: Nitrogen fixation-enhanced carbon sequestration in low nitrate, low chlorophyll seascapes, *Mar. Ecol. Prog. Ser.*, 354, 257–268, doi:10.3354/meps07547, 2008.
- Kohonen, T.: Self-Organizing Maps. Third, extended edition, Springer-Verlag, Berlin, Heidelberg, New York, 501 pp., 2001.
- Kurihara, Y., Sakurai, T., and Kuragano, T.: Global daily sea surface temperature analysis using data from satellite microwave radiometer, satellite infrared radiometer and in-situ observations, *Sokko-jiho*, 73, S1–S18, 2006.
- Lefèvre, N., Watson, A. J., and Watson, A. R.: A comparison of multiple regression and neural network techniques for mapping in situ $p\text{CO}_2$ data, *Tellus*, 57B, 375–384, doi:10.1111/j.1600-0889.2005.00164.x, 2005.
- Lin, I.-I., Hu, C., Li, Y.-H., Ho, T.-Y., Fischer, T. P., Wong, G. T. F., Wu, J., Huang, C.-W., Allen Chu, D., Ko, D. S., and Chen, J.-P.: Fertilization Potential of Volcanic Dust in the Low-Nutrient Low-Chlorophyll Western North Pacific Subtropical Gyre: Satellite Evidence and Laboratory Study, *Global Biogeochem. Cy.*, 25, GB1006, doi:10.1029/2009GB003758, 2011.

- Lewis, E. and Wallace, D. W. R.: Program Developed for CO_2 System Calculations. ORNL/CDIAC-105. Carbon Dioxide Information Analysis Center, Oak Ridge National Laboratory, U.S. Department of Energy, Oak Ridge, Tennessee, doi:10.3334/CDIAC/otg.CO2SYS_DOS_CDIAC105, 1998.
- Midorikawa, T., Ishii, M., Nemoto, K., Kamiya, H., Nakadate, A., Masuda, S., Matsueda, H., Nakano, T., and Inoue, H. Y.: Interannual variability of winter oceanic CO_2 and air-sea CO_2 flux in the western North Pacific for 2 decades, *J. Geophys. Res.*, 111, C07S02, doi:10.1029/2005JC003095, 2006.
- Miller, L. A., Christian, J., Davelaar, M., Johnson, W. K., and Linguanti, J.: Carbon Dioxide, Hydrographic and Chemical Data Obtained During the Time Series Line P Cruises in the North-East Pacific Ocean from 1985–2010, http://cdiac.ornl.gov/ftp/oceans/CLIVAR/Line_P.data/, Carbon Dioxide Information Analysis Center, Oak Ridge National Laboratory, US Department of Energy, Oak Ridge, Tennessee, doi:10.3334/CDIAC/otg.CLIVAR_Line_2009, 2010.
- Murphy, P. P., Nojiri, Y., Fujinuma, Y., Wong, C. S., Zeng, J., Kimoto, T., and Kimoto, H.: Measurements of Surface Seawater $f\text{CO}_2$ from Volunteer Commercial Ships: Techniques and Experiences from Skaugran, *J. Atmos. Ocn. Tech.*, 18, 1719–1734, 2001a.
- Murphy, P. P., Nojiri, Y., Harrison, D. E., and Larkin, N. K.: Scales of spatial variability for surface ocean $p\text{CO}_2$ in the Gulf of Alaska and Bering Sea: toward a sampling strategy, *Geophys. Res. Lett.*, 28, 1047–1050, 2001b.
- Olsen, A., Bellerby, R. G. J., Johannessen, T., Omar, A., and Skjelvan, I.: Interannual variability in the wintertime air-sea flux of carbon dioxide in the northern North Atlantic, 1981–2001, *Deep-Sea Res. I*, 50, 1323–1338, 2003.
- O'Reilly, J. E., Maritorena, S., Siegel, D., O'Brien, M. C., Toole, D., Mitchell, B. G., Kahru, M., Chavez, F. P., Strutton, P., Cota, G., Hooker, S. B., McClain, C. R., Carder, K. L., Muller-Karger, F., Harding, L., Magnuson, A., Phinney, D., Moore, G. F., Aiken, J., Arrigo, K. R., Letelier, R., and Culver, M.: Ocean color chlorophyll a algorithms for SeaWiFS, OC_2 , and OC_4 : Version 4, in: *SeaWiFS Postlaunch Technical Report Series*, edited by: Hooker, S. B. and Firestone, E. R., Vol. 11, *SeaWiFS Postlaunch Calibration and Validation Analyses, Part 3*. NASA, Goddard Space Flight Center, Greenbelt, Maryland, 9–23, 2000.
- Patra, P. K., Maksyutov, S., Ishizawa, M., Nakazawa, T., Takahashi, T. and Ukita, J.: Interannual and decadal changes in the sea-air CO_2 flux from atmospheric CO_2 inverse modeling, *Global Biogeochem. Cy.*, 19, GB4013, doi:10.1029/2004GB002257, 2005.
- Pfeil, B., Olsen, A., Bakker, D. C. E., Hankin, S., Koyuk, H., Kozyr, A., Malczyk, J., Manke, A., Metzl, N., Sabine, C. L., Akl, J., Alin, S. R., Bellerby, R. G. J., Borges, A., Boutin, J., Brown, P. J., Cai, W.-J., Chavez, F. P., Chen, A., Cosca, C., Fassbender, A. J., Feely, R. A., González-Dávila, M., Goyet, C., Hardman-Mountford, N., Heinze, C., Hood, M., Hoppema, M., Hunt, C. W., Hydes, D., Ishii, M., Johannessen, T., Jones, S. D., Key, R. M., Körtzinger, A., Landschützer, P., Lauvset, S. K., Lefèvre, N., Lenton, A., Lourantou, A., Merlivat, L., Midorikawa, T., Mintrop, L., Miyazaki, C., Murata, A., Nakadate, A., Nakano, Y., Nakaoka, Y., Nojiri, A. M., Omar, X. A., Padin, G.-H., Park, K., Paterson, F. F., Perez, S., Pierrot, D., Poisson, A., Ríos, A. F., Salisbury, J., Santana-Casiano, J. M., Sarma, V. V. S. S., Schlitzer, R., Schneider, B., Schuster, U., Sieger, R., Skjelvan, I., Steinhoff, T., Suzuki, T., Takahashi, T., Tedesco, K., Telszewski, M., Thomas, H., Tilbrook, B., Tjiputra, J., Vandemark, D., Veness, T., Wanninkhof, R., Watson, A. J., Weiss, R., Wong, C. S., and Yoshikawa-Inoue, H.: A uniform, quality controlled Surface Ocean CO_2 Atlas (SOCAT), *Earth Syst. Sci. Data*, 5, 125–143, doi:10.5194/essd-5-125-2013, 2013.
- Robbins, L. L., Hansen, M. E., Kleypas, J. A., and Meylan, S. C.: CO_2calc – A user-friendly seawater carbon calculator for Windows, Max OS X, and iOS (iPhone): U.S. Geological Survey Open-File Report 2010–1280, p. 17, 2010.
- Sabine, C. L., Feely, R. A., Gruber, N., Key, R. M., Lee, K., Bullister, J. L., Wanninkhof, R., Wong, C. S., Wallace, D. W. R., Tilbrook, B., Millero, F. J., Peng, T.-H., Kozyr, A., Ono, T., and Rios, A. F.: The Oceanic Sink for Anthropogenic CO_2 , *Science*, 305, 367–371, doi:10.1126/science.1097403, 2004.
- Sabine, C. L., Maenner, S., and Sutton, A.: High-resolution ocean and atmosphere $p\text{CO}_2$ time-series measurements from mooring Papa_145W_50N, Carbon Dioxide Information Analysis Center, Oak Ridge National Laboratory, US Department of Energy, Oak Ridge, Tennessee, doi:10.3334/CDIAC/otg.TSM_Papa_145W_50N, 2010.
- Sabine, C. L., Hankin, S., Koyuk, H., Bakker, D. C. E., Pfeil, B., Olsen, A., Metzl, N., Kozyr, A., Fassbender, A., Manke, A., Malczyk, J., Akl, J., Alin, S. R., Bellerby, R. G. J., Borges, A., Boutin, J., Brown, P. J., Cai, W.-J., Chavez, F. P., Chen, A., Cosca, C., Feely, R. A., González-Dávila, M., Goyet, C., Hardman-Mountford, N., Heinze, C., Hoppema, M., Hunt, C. W., Hydes, D., Ishii, M., Johannessen, T., Key, R. M., Körtzinger, A., Landschützer, P., Lauvset, S. K., Lefèvre, N., Lenton, A., Lourantou, A., Merlivat, L., Midorikawa, T., Mintrop, L., Miyazaki, C., Murata, A., Nakadate, A., Nakano, Y., Nakaoka, S., Nojiri, Y., Omar, A. M., Padin, X. A., Park, G.-H., Paterson, K., Perez, F. F., Pierrot, D., Poisson, A., Ríos, A. F., Salisbury, J., Santana-Casiano, J. M., Sarma, V. V. S. S., Schlitzer, R., Schneider, B., Schuster, U., Sieger, R., Skjelvan, I., Steinhoff, T., Suzuki, T., Takahashi, T., Tedesco, K., Telszewski, M., Thomas, H., Tilbrook, B., Vandemark, D., Veness, T., Watson, A. J., Weiss, R., Wong, C. S., and Yoshikawa-Inoue, H.: Surface Ocean CO_2 Atlas (SOCAT) gridded data products, *Earth Syst. Sci. Data*, 5, 145–153, doi:10.5194/essd-5-145-2013, 2013.
- Sarma, V. V. S. S., Saino, T., Sasaoka, K., Nojiri, Y., Ono, T., Ishii, M., Inoue, H. Y., and Matsumoto, K.: Basin-scale $p\text{CO}_2$ distribution using satellite sea surface temperature, Chl-a, and climatological salinity in the North Pacific in spring and summer, *Global Biogeochem. Cy.*, 20, GB3005, doi:10.1029/2005GB002594, 2006.
- Schmitz, W. J. Jr.: *On the World Ocean Circulation: Volume I; Some Global Features/North Atlantic Circulation*, edited by: Rept., Tech., Woods Hole Oceanogr. Inst., Woods Hole, Massachusetts 02543, 1996.
- Schuster, U., Watson, A. J., Bates, N. R., Corbière, A., González-Dávila, M., Metzl, N., Pierrot, D., and Santana-Casiano, M.: Trends in North Atlantic sea-surface $f\text{CO}_2$ from 1990 to 2006, *Deep-Sea Res. II*, 56, 620–629, 2009.
- Stephens, M. P., Samuels, G., Olson, D. B., Fine, R. A., and Takahashi, T.: Sea-air flux of CO_2 in the North Pacific using shipboard and satellite data, *J. Geophys. Res.*, 100, 13571–13583, 1995.
- Takahashi, T., Olafsson, J., Godard, J. G., Chipman, D. W., and Sutherland, S. C.: Seasonal variation of CO_2 and nutrient in the

- high-latitude surface oceans: A comparative study, *Global Biogeochem. Cy.*, 7, 843–878, 1993.
- Takahashi, T., Sutherland, S. C., Feely, R. A., and Wanninkhof, R.: Decadal change of the surface water $p\text{CO}_2$ in the North Pacific: A synthesis of 35 years of observations, *J. Geophys. Res.*, 111, C07S05, doi:10.1029/2005JC003074, 2006.
- Takahashi, T., Sutherland, S. C., Wanninkhof, R., Sweeney, C., Feely, R. A., Chipman, D. W., Hales, B., Friederich, G., Chavez, F., Watson, A., Bakker, D. C. E., Schuster, U., Metzl, N., Inoue, H. Y., Ishii, M., Midorikawa, T., Sabine, C. L., Hopemma, M., Olafsson, J., Arnarson, T. S., Tilbrook, B., Johannessen, T., Olsen, A., Bellerby, R., de Baar, H. J. W., Nojiri, Y., Wong, C. S., and Delille, B.: Climatological mean and decadal change in surface ocean $p\text{CO}_2$, and net sea-air CO_2 flux over the global oceans, *Deep-Sea Res. II*, 56, 554–577, doi:10.1016/j.dsr2.2008.12.009, 2009.
- Takamura, T. R., Inoue, H. Y., Midorikawa, T., Ishii, M., and Nojiri, Y.: Seasonal and inter-annual variations in $p\text{CO}_2$ sea and air-sea CO_2 fluxes in mid-latitudes of the western and eastern North Pacific during 1999–2006: Recent results utilizing voluntary observation ships, *J. Meteorol. Soc. Japan*, 88, 883–898, doi:10.2151/jmsj.2010-602, 2010.
- Telszewski, M., Chazottes, A., Schuster, U., Watson, A. J., Moulin, C., Bakker, D. C. E., González-Dávila, M., Johannessen, T., Körtzinger, A., Lüger, H., Olsen, A., Omar, A., Padin, X. A., Ríos, A. F., Steinhoff, T., Santana-Casiano, M., Wallace, D. W. R., and Wanninkhof, R.: Estimating the monthly $p\text{CO}_2$ distribution in the North Atlantic using a self-organizing neural network, *Biogeosciences*, 6, 1405–1421, doi:10.5194/bg-6-1405-2009, 2009.
- Trenberth, K. E. and Caron, J. M.: The Southern Oscillation revisited: Sea level pressures, surface temperatures and precipitation, *J. Climate*, 13, 4358–4365, 2000.
- Usui, N., Ishizaki, S., Fujii, Y., Tsujino, H., Yasuda, T., and Kamachi, M.: Meteorological Research Institute multivariate ocean variational estimation (MOVE) system: Some early results, *Adv. Space Res.*, 37, 806–822, doi:10.1016/j.asr.2005.09.022, 2006.
- Valsala, V., Maksyutov, S., Telszewski, M., Nakaoka, S., Nojiri, Y., Ikeda, M., and Murtugudde, R.: Climate impacts on the structures of the North Pacific air-sea CO_2 flux variability, *Biogeosciences*, 9, 477–492, doi:10.5194/bg-9-477-2012, 2012.
- Wakita, M., Watanabe, S., Murata, A., Tsurushima, N., and Honda, M.: Decadal change of dissolved inorganic carbon in the subarctic western North Pacific Ocean, *Tellus B*, 62, 608–620, doi:10.1111/j.1600-0889.2010.00476.x, 2010.
- Wong, C. S. and Johannessen, S.: Sea surface and atmospheric $p\text{CO}_2$ data in the Pacific Ocean during the station P cruises from 1973–2003., Carbon Dioxide Information Analysis Center, Oak Ridge National Laboratory, US Department of Energy, Oak Ridge, Tennessee, doi:10.3334/CDIAC/otg.VOS_station_p_ca, 2010.
- Wong, C. S., Christian, J. R., Emmy Wong, S.-K., Page, J., Xie, L., and Johannessen, S.: Carbon dioxide in surface seawater of the eastern North Pacific Ocean (Line P), 1973–2005, *Deep-Sea Res. I*, 57, 687–695, doi:10.1016/j.dsr.2010.02.003, 2010.
- Zeng, J., Nojiri, Y., Murphy, P. P., Wong, C. S., and Fujinuma, Y.: A comparison of $\Delta p\text{CO}_2$ distributions in the northern North Pacific using results from a commercial vessel in 1995–1999, *Deep-Sea Res. II*, 49, 5303–5315, 2002.